ELSEVIER

Journal of Fluids and Structures 26 (2010) 544–558

JOURNAL OF FLUIDS AND STRUCTURES

www.elsevier.com/locate/jfs

Experimental investigation of the effect of chordwise flexibility on the aerodynamics of flapping wings in hovering flight

K. Mazaheri, A. Ebrahimi*

Aerospace Systems Center of Excellence, Sharif University of Technology, Tehran, Iran

Received 6 January 2009; accepted 2 March 2010
Available online 10 April 2010

Abstract

Ornithopters or mechanical birds produce aerodynamic lift and thrust through the flapping motion of their wings. Here, we use an experimental apparatus to investigate the effects of a wing's twisting stiffness on the generated thrust force and the power required at different flapping frequencies. A flapping wing system and an experimental set-up were designed to measure the unsteady aerodynamic and inertial forces, power usage and angular speed of the flapping wing motion. A data acquisition system was set-up to record important data with the appropriate sampling frequency. The aerodynamic performance of the vehicle under hovering (i.e., no wind) conditions was investigated. The lift and thrust that were produced were measured for different flapping frequencies and for various wings with different chordwise flexibilities. The results show the manner in which the elastic deformation and inertial flapping forces affect the dynamical behavior of the wing. It is shown that the generalization of the actuator disk theory is, at most, only valid for rigid wings, and for flexible wings, the power P varies by a power of about 1.0 of the thrust T. This aerodynamic information can also be used as benchmark data for unsteady flow solvers.

Keywords: Flapping wing; Flexible membrane wing; Hovering flight

1. Introduction

In recent years, flight by mechanical flapping wings has gained significant interest. An important advantage of flapping wing propulsion is that lift can be generated with little or no forward velocity and with a small wing size. This is driven by the notion that flapping wings at small scales may offer some unique aerodynamic advantages over traditional fixed and rotary wing modes of propulsion (Sibilski et al., 2007). Flapping wing flight more closely mimics natural flight and has the potential for lower weight and greater endurance. Thus, one of the goals of studying flapping flight is to scale to a micro air vehicle (MAV) class. These vehicles are capable of performing a wide range of possible military and civilian missions. The most important usage of MAVs is in reconnaissance, imperceptible guarding and surveillance, which requires a slow flight and excellent maneuverability (Bruce, 1997; Mazaheri et al., 2007).

The propulsion system of an ornithopter (flapping wing aircraft configuration) consists of different components including a battery, an electric motor, a gearbox, a flapping mechanism and flexible wings. For designing ornithopter systems, the most significant subsystem is the flexible wing. Although natural selection in birds and insects over millions of years has optimized the materials, components, configurations and kinematics of their wings, we must optimize this subsystem by 3D unsteady flow simulations and experimental studies of flapping flight (Mazaheri et al., 2008).

*Corresponding author. Tel./fax: +98 21 66022731.
E-mail address: ebrahimi_a@ae.sharif.edu (A. Ebrahimi).

0889-9746/$ - see front matter © 2010 Elsevier Ltd. All rights reserved.
doi:10.1016/j.jfluidstructs.2010.03.004

Studies to date on the aerodynamics of flapping flight, although beneficial to an understanding of the subject, have not taken into account all of the details that are necessary to obtain a complete and thorough understanding. For the same reason, no design method for flapping wings is readily available (Shyy et al., 1999).

Although many researchers have noted that flexible wings play an important role in the aerodynamics of flapping flight, there exist very few, although important, studies dealing with flexible rather than rigid wings in flapping flight (Smith, 1996; Daniel and Combes, 2002; Combes and Daniel, 2003; Ho et al., 2003; Maglasang et al., 2006). Numerical and experimental work thus far has centered on rigid wings because the aeroelastic interaction between the wing and surrounding fluid can then be neglected and the overall complexity of the problem is greatly reduced. However, the computational means and fluid mechanical analyses have advanced to the point at which the aeroelastic interaction can now be included (Isogai and Harino, 2007).

The design of a flapping wing vehicle for slow forward flight requires knowledge of how a highly flexible wing will deform under aerodynamic loading and the effect of that deformation on wing efficiency. The temporal shape of the wing itself depends upon many physical parameters such as camber, chord and span length and, most importantly, the mass and stiffness distribution. However, dynamic quantities such as the time-dependent pressure loading, wing speed, free stream velocity and local acceleration of the wing surface also directly drive the instantaneous wing deformation. Therefore, it is the dynamic coupling between the wings and surrounding air that determines the final lift and thrust force. This poses an interesting question: can a manipulation of the wing's aeroelastic properties lead to improved performance? Clearly, changes in the wing deformation will affect the aerodynamics, and so it seems quite possible that changes in the physical properties of the wing could yield better performance. In many respects, this is an inverse problem, where the desired result is known, but not the wing shape or structure needed to achieve it (Ho et al., 2003).

Flight power has become the key component for the quantification of flight performance (Shyy et al., 1999; Frampton et al., 2002). Sibilski et al. (2007) used the modified strip theory and modified panel method aerodynamic models to estimate the mechanical power output for complex, unsteady flows of flapping flight.

In this study, a mechanical flapping system, capable of producing flapping motion, was designed and built. Flexible membrane-type wings are used. Typical biological aviators have several degrees of freedom with which they manipulate their wings. Our goal was to achieve a similar wing manipulation with only a single degree of freedom. This is accomplished by tuning the wing twisting stiffness through changing the chordwise rib thicknesses. The effect of wing flexibility on the aerodynamic forces of lift and thrust were explored and observed. The aerodynamic performance of the vehicle for a hovering (i.e., no wind) situation was investigated. The produced lift and thrust were measured for different wings and different flapping frequencies, and we show how the elastic deformation and inertial flapping forces affect the dynamical behavior of the wings. Here, a pitching deformation is passively produced by the interaction of the flapping motion and the inertial and aeroelastic characteristics of the wings. These results can be used in designing an improved flapping machine wing design. This information can also be used for the validation of unsteady flow simulations needed for the engineering design of ornithopters, which we are currently carrying out as an independent research topic.

2. Specification of the TADBIR ornithopter

An ornithopter called TADBIR, as shown in Fig. 1, is used here. The basic design of this ornithopter was presented by Ebrahimi et al. (2005), Ebrahimi and Mazaheri (2006) and Mazaheri et al. (2008). This system consists of a main frame, one tail and two flexible membrane wings, a quasi-symmetric four-bar flapping mechanism, a gearbox, a very small DC electrical motor, a lithium-polymer battery, a receiver, a speed controller, two servos (for tail horizontal and vertical movements) and a transmitter. Ornithopters need a fairly high power-to-weight ratio. Efficient electric motors are usually designed for a low torque and high angular velocity, and a gearbox is needed to decrease the angular speed to flapping frequencies. This system contains two planar four-bar mechanisms (to transform the rotational motion to a flapping motion) connected to the DC engine through a gearbox. The TADBIR ornithopter's wing span is 80 cm, and its average chord length is 14 cm. It is capable of flapping its flexible membrane wing at a maximum frequency of 10 Hz. The specifications of this system are summarized in Table 1. The aerodynamic forces are generated by the nonsymmetrical motion of the wings. This system has shown to have the ability for level flight, rapid climbing, quick dives and circle maneuvers.

3. Flapping wing mechanism

The flapping mechanism was adapted from a Cybird P1 remotely controlled ornithopter (Kim et al., 2003). This four-bar mechanism transforms the rotational motion of an electric motor to a flapping motion. In our experimental set-up,

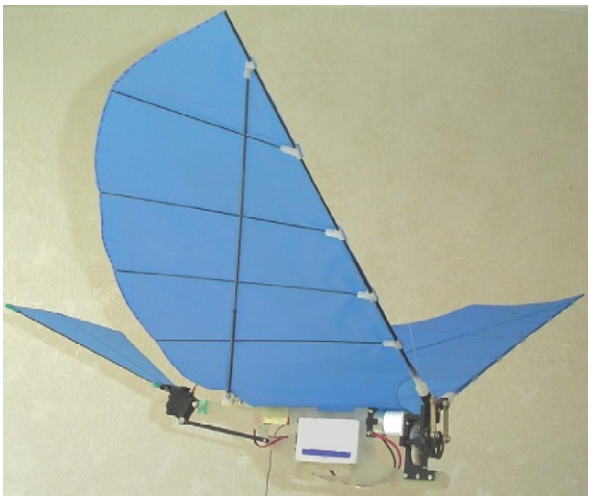

Fig. 1. TADBIR Ornithopter.

Table 1
Specifications of TADBIR ornithopter.

Parameter	Specification
Wing span (cm)	80
Wing aspect ratio	6
Upstroke angle (deg)	30
Downstroke angle (deg)	19
Flapping frequency (Hz)	0–10
Body length (cm)	35
Propulsion system	DC motor/battery
Weight (g)	230

the driving motor is powered directly by a DC power supply, although in principle, it could be powered by batteries. The flapping frequency is controlled directly by altering the input voltage. The motor nominal voltage is 7.2 V DC with a stall torque of 36.3 mN m. The motor is geared down by a ratio of 24:1 to lower speeds and provides sufficient torque to drive the wings. Fig. 2(a) shows the flapping mechanism used in the experiment and the range of operating angles of the flapping mechanism. The follower link oscillates between $+30^\circ$ and -19° from the horizontal line. Note that these values are real measured values and include tolerance effects, while the values based on our analytical model (Mazaheri et al., 2008) are between $+29^\circ$ and -21°. Since the wing structure is flexible, and due to inertial forces, the operating angle of the flexible wing is different and depends on the wing length, the material and the flapping frequency. At high frequencies, the span-wise flexibility may result in large deformation in the span direction of each wing, as high as 30 (see Fig. 2(b)). During the test, the flapping mechanism is capable of flapping at a maximum frequency of 10 Hz. The wing's leading edge is rigidly attached to the follower link of the mechanism, and the trailing edge has a phase delay with respect to the motion of the leading edge.

The normal flapping motion, which occurs when a constant voltage is applied to the motor, results in different upstroke and downstroke periods. Here, the kinematics of the flapping mechanism has been modeled. Fig. 3 shows analytical results for the angular displacement and the corresponding velocity and acceleration of the follower link versus time, for a full period of flapping. In this figure, the upstroke starts at 5° above the horizontal plane and continues until 29°. The downstroke follows, up to 21° below the horizontal plane. The maximum angular velocity is about 15 rad/s and occurs close to the horizontal plane. Obviously, the angular velocity is equal to zero at both ends of the up and downstrokes. In this analysis, the angular velocity of the motor is assumed to be constant.

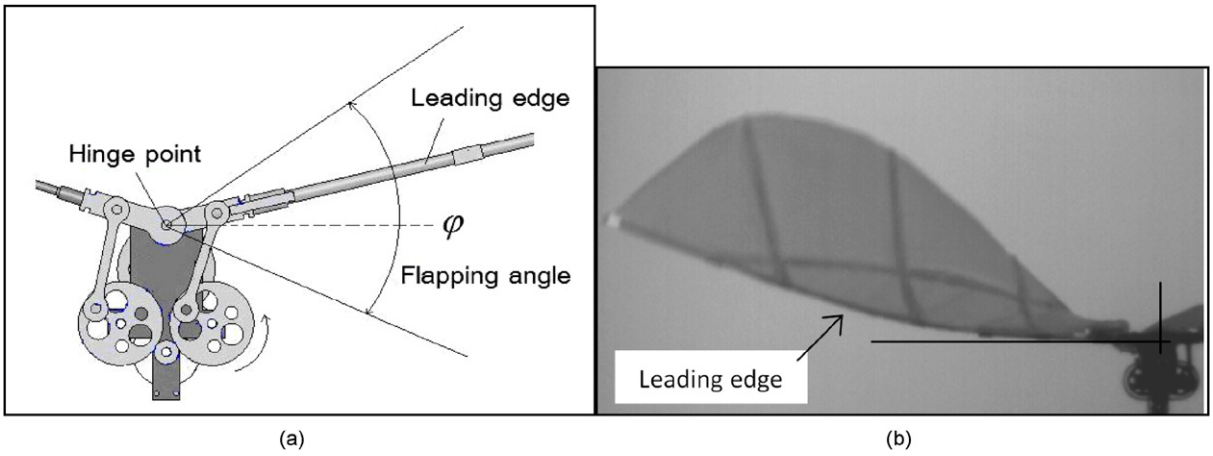

Fig. 2. (a) The flapping wing mechanism and (b) a snapshot of high speed camera (front view).

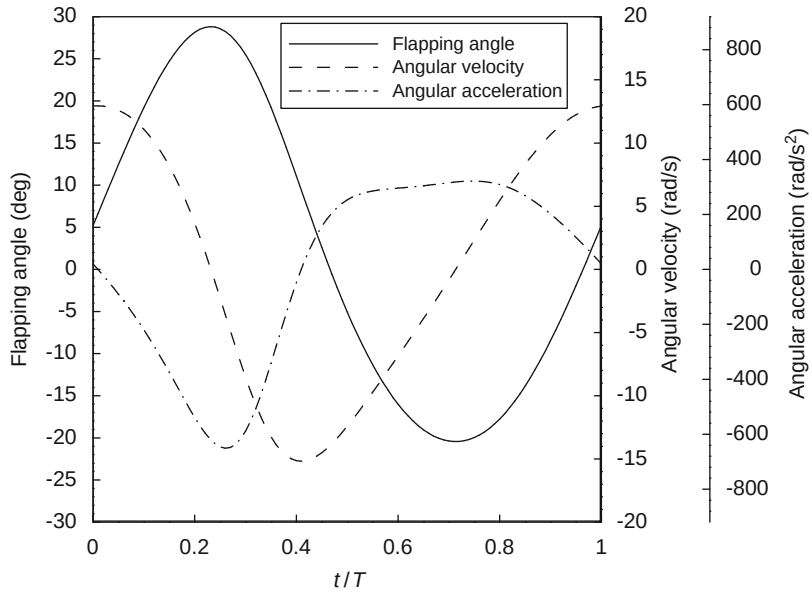

Fig. 3. Analytical results for flapping angle, angular flapping velocity and angular flapping acceleration for one complete cycle (5.1 Hz frequency).

4. Flexible wing development

Returning to the biological motivation for flapping flight, note that birds are not limited to a fixed wing kinematic motion, but instead can change their wings' kinematic motion to gain the most advantageous geometry when maneuvering or transitioning from one flight mode to another. Mechanical flappers do not have as many degrees of freedom as natural flyers. The simplest way to have variable wing kinematics is through a rotary DC motor connected to a four-bar mechanism through a gearing system. By varying the structural stiffness of the wing, one may affect the aeroelastic performance of the wing. This change in wing shape and velocity will cause changes in the generation, growth rate and shedding of the unsteady leading edge vortex over the entire wing. One could attempt to experimentally find the optimum configuration by examining different wing designs.

The objective of this research is to develop aeroelastic wings by understanding the effect of wing flexibility on the resulting aerodynamic load generation. Finally, we hope to find an optimal thrust-to-power ratio, which is an index of wing efficiency. This efficiency is strongly dependent on temporal and spatial wing deformation and the phase lag between translational and torsional wing articulation. The primary objective is therefore to investigate how different designs differ in this regard and to find the optimal configuration with optimal aerodynamic forces. A few different wings were constructed, with different structural designs. However, the articulation of these wings is constrained to a single degree of freedom, i.e., the wing's root movement. Therefore, the most desirable articulation is achieved through passive elastic characteristics. We believe that changes in the design affect elastic performance in the span and chord directions, and a better force generation is the result of a better tuning between different elastic modes.

Fig. 4 shows the structure of the flexible membrane wings developed here, for two different types. Here, five wings of type A were constructed with a similar planform in order to preserve the geometric similarity. The geometrical characteristics of the wings and the mechanical properties of the materials used are shown in Tables 2 and 3. The wing's cover is made of a 0.05-mm-thick nylon sheet and is stiffened by carbon-fiber "ribs". One rib constructs the leading edge of the wing as the main spar, while three other ribs run in the chord direction. A planform view of the wing's shape and an image of the constructed wing are shown in Fig. 5. The primary variables in the wing design are the width and thickness of the stiffeners in the chord direction. By varying these parameters, the twisting characteristics can be tuned over a wide range. The leading edge of the wing root is attached to the follower link of the flapping mechanism (see Fig. 5). These wings have a roughly half-elliptical planform with a span of 80–100 cm and an aspect ratio of 5.7–6.8.

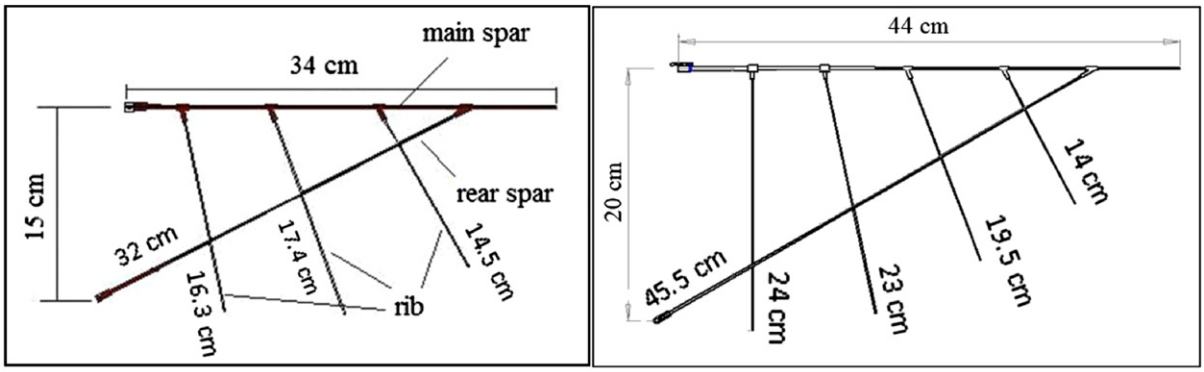

Fig. 4. Flexible membrane wing structure used in the experiments.

Table 2
Characteristics of the wing used in these experiments.

Wing type	Semi-span (cm)	Mean chord (cm)	Single wing area (cm^2)	Mass (g)	Rod thickness (mm)		
					Main spar	Rear spar	Rib
A1–A5	40	14	470	13.9–19.3	2	1.5	0.7–4.0
B	50	17	880	20.8	1.6	1.4	1

Table 3
Mechanical properties of the wing's material used in these experiments.

Materials	Density (kg/m^3)	Young's modulus (Gpa)	Poisson's ratio
Carbon rod	1400	133	0.28
Wing cover	1200	4.0	–

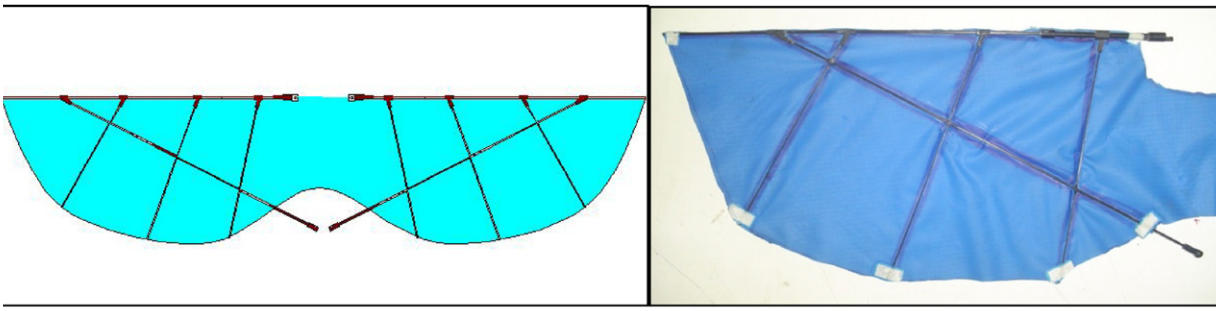

Fig. 5. (a) A planform view of the wing's shape schematic and (b) picture of the constructed wing.

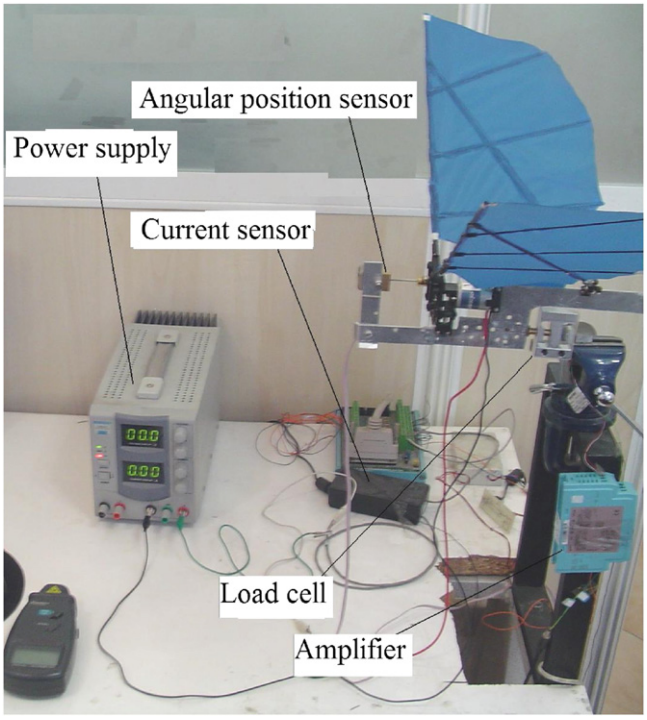

Fig. 6. Experimental set-up.

5. Experimental set-up

A test bed, as shown in Fig. 6, was built to investigate the wings' aeroelastic characteristics. This set-up measures the instantaneous lift and thrust forces and the flapping power usage. Six different wings were constructed with different chordwise stiffness values and were tested to compare their dynamic performance. The rig consisted of a flapping mechanism powered by a low inertia DC motor to create flapping motions with pre-selected amplitudes. The flapping frequency could be controlled. Instantaneous unsteady lift and thrust forces data were measured using a one-dimensional load cell (FUTEK model L2330). The load cell was installed in the proper direction to measure horizontal and vertical forces, respectively. The load cell was calibrated using known weights, and the measured calibration factors were used to convert the gauge voltage signals to forces. The signals received from the strain gauges were amplified electronically using an ADAMS 3016 amplifier, before being sampled at 1000 Hz.

A system of four Hall sensors was integrated, installed and calibrated to measure the angular position, angular speed and flapping frequency of the wing root. This sensor was directly attached to the flapping link, so the angular position is

directly measured, and the other information is found by processing this data. To measure the wing's power usage, a measuring unit was designed to use the CSNE151-100 closed loop current sensor.

All signals were acquired using an Advantech data acquisition board (model PCI 1710 HG) in a PC running custom-designed software written in MATLAB. A specially written MATLAB routine controls the entire process. The data acquisition process starts by calculating the forces, power usage and flapping angle (motor shaft position) using the calibration factors. Then, the data is filtered in an on-line process using a third-order low-pass digital Butterworth filter with a cut-off frequency of about 15 Hz. This cut-off frequency will filter the high frequency noises generated by motor jitter or other component vibrations. We assume that the high frequency oscillations are not related to the dynamics or aerodynamics of the wings. The first natural frequency of the wings is much higher than the flapping frequencies considered here.

A high speed camera was used to visualize the movement of our fast deforming wings, by recording up to 1000 high resolution frames per second. To understand the physical correlations between the wing mechanical deformation and the generated aerodynamic forces, wing aerodynamic force data and other signals were synchronized with the high speed video recordings. This helps us to better understand the effects of different physical phenomena on the measured quantities, which otherwise are not easy to explain. In addition, we note that the position sensors will only show the location of the wing main spar root, while there could be an enormous bending in this spar and the whole wing surface (see Fig. 2(b)).

6. Experimental uncertainty

To analyze the uncertainty and repeatability of our experiments, we first discuss the error margins for each sensor, and then explain how we used a few tests to assess the uncertainty. For the load cell, a random static loading measurement in the range of up to 1000 g shows that the relative error is below 0.5%. The hysteresis, nonrepeatability and nonlinearity of this sensor are below 0.1%. The natural frequency of this sensor is well above our flapping frequencies. Our Hall sensors have an absolute error of 1°. The current sensor is appropriate for variable speed drives and measures AC or DC current with 0.5% accuracy.

The A/D system used to collect the force measurement data has a resolution of 12 bits over a range of ± 10 V, giving an accuracy of 0.08% FSR ± 1 LSB. The electrical wires were properly shielded, and other recommended practices were followed as much as possible to reduce noise. A low-pass digital Butterworth filter with an appropriate cut-off frequency was used to increase the signal-to-noise ratio.

The measurements were performed up to six times to verify the repeatability, and to estimate the experimental uncertainty. Uncertainties in force and power measurements were experimentally determined to be less than 2.5% and 1.3%, respectively.

7. Scaling parameters and procedure

Two main dimensionless parameters in flapping-flight scaling can be used to study the performance of a hovering flapping rigid wing: (i) the Reynolds number, which represents a ratio of inertial and viscous forces and (ii) the reduced frequency, which describes the rotational versus translational speeds during flapping movement. Together with geometric and kinematic similarities, the Reynolds number and the reduced frequency are sufficient to define the aerodynamic similarity for a rigid wing (Maybury and Lehmann, 2004; Isaac et al., 2006; Shyy et al., 2008).

Using v, the fluid kinematic viscosity, the mean chord length c_m as the reference length and the mean wingtip velocity as the reference velocity, $U_{\mathrm{ref}} = 2\varphi fR$, where φ is the wing-beat amplitude as shown in Fig. 2(a), measured in radians, f is the flapping frequency and R is the wing length (half wing span), the Reynolds number for a 3-D flapping wing in hovering flight can be cast as (Ellington, 1999)

$$\mathrm{Re} = \frac{2\varphi fRc_m}{v} = \left(\frac{4}{\mathrm{AR}}\right)\frac{\varphi fR^2}{v},$$

where the aspect ratio AR is introduced in the form $\mathrm{AR} = (2R)^2/S$, with the wing area (S) being the product of the wing span ($2R$) and the mean chord length (c_m).

In hovering flight, for which there is no forward speed, the reference speed U_{ref} is defined as the mean wingtip velocity and the reduced frequency can be rewritten as

$$k = \frac{\pi fL_{\mathrm{ref}}}{U_{\mathrm{ref}}} = \frac{\pi c_m}{2\varphi R} = \frac{\pi}{\varphi AR}.$$

Note that the wing-beat frequency, f, does not appear explicitly in the reduced frequency. This analysis shows that for hovering flight with a rigid flapping wing, two geometrically and kinematically similar flapping wings need only have similar fR^2 values to have similar force coefficients. However, we have observed that for a flexible wing this is not applicable. This can be observed in the results presented in this paper.

Many light flexible membrane wings with different designs were fabricated to perform these tests. The main structures of the wings were constructed from a fairly stiff leading edge main spar and flexible ribs attached to the main spar. This structure is covered by a light and thin fabric. Here, we present results for six different wings and two different types (A and B, introduced in Table 2). The wings' planforms are semi-elliptical with an aspect ratio of 5.7–6.8. Additionally, a flapping mechanism was designed and fabricated to generate controlled-frequency flapping motion. The flapping frequencies vary from 2 to 7 Hz, and the wing-beat amplitude (see Fig. 2(a)) is $\varphi = 49^\circ$. In our experiments, the flapping frequency and the AR of the wing are variable and result in Re numbers ranging from 10^4 to 5×10^4 and reduced frequencies ranging from $k = 0.54$ (type A) to $k = 0.64$ (type B).

The generated lift, thrust and power consumption were measured in each case. The graphs presented here show the temporal variation and time average of the measured data.

The objective of these experiments is to investigate how different designs and parameters affect the generated aerodynamic forces and the consumed energy. In addition, we would like to find an optimum combination of wing flexibility and thrust generation. One may note that a rigid wing will not produce any net lift or thrust, while a suitable flexibility and deformation will produce the maximum aerodynamic forces by utilizing the smallest amount of energy.

8. Results and discussion

8.1. Total normal force

Many researchers have investigated flow structures around flapping wings (Ho et al., 2003; Maybury and Lehmann, 2004; Heathcote et al., 2004; Poelma et al., 2006; Shyy et al., 2008). Most of these studies are numerical. Authors have also extensively used the simple strip theory and lattice method solvers to understand pressure variations and complex vortical flows around flapping wings. Extensive results have been reported by Ebrahimi and Mazaheri (2006), Ebrahimi and Mazaheri (2008). However, it has not yet been possible to consider elastic deformations in our aerodynamic computations (although it is being pursued). Of course, in high frequency flapping, one would expect significant differences due to flexibility effects on aerodynamic forces.

Here, we present the results of our experimental investigation of the normal force of hovering flexible flapping wings. In two subsequent tests, the load cell measures two components of the aerodynamic forces, one in the axial direction, called the thrust, and the other force, normal to it, called the normal force. This normal force was measured for wing 2 type A, and the results are shown in Fig. 7, including wing angular position, angular velocity and the normal force. Note that the normal force is a combination of the aerodynamic and inertial forces. In fact, here, we measure the dynamic response of the load cell to the whole system of the flapping wing and its stand. The periodic trend in Fig. 7 is the same for all of the wings and frequencies investigated. We did not observe the high frequency force component reported by Hong (2006), and we propose that this is due to the high level of noise in their data acquisition system. Additionally, we note that the normal force has a phase shift with respect to the wing movement, which is due to the lag in the elastic deformation caused by the inertial forces. Fig. 7 shows that

(i). the normal force has a phase shift of about 20° with respect to the flapping angle and is positive for most of the downstroke and negative otherwise; the maximum occurs close to the middle of the flapping angles (-19° and $+30^\circ$), which corresponds to $+6^\circ$, where the flapping velocity is maximum;
(ii). for a very short time during the end of the upstroke, the lift force is positive, and a similar phenomenon is observed for the downstroke.

The high speed camera shows that the trailing edge of the wing has a phase lag with respect to the follower link of the four-bar mechanism (see Fig. 2(b)). This lag is mostly effective at the end and beginning of each stroke.

8.2. Inertial forces

The total normal force has two components: the inertial force, which is a function of the wing mass distribution and the flapping kinematics, and the aerodynamic force caused by the flapping motion and wing deformation (Maybury and

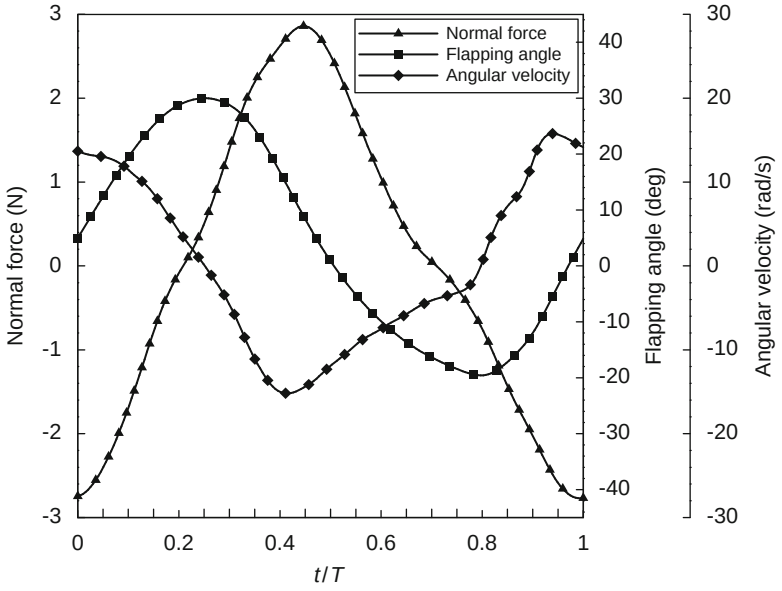

Fig. 7. The total normal force variation for wing A2 (5.1 Hz frequency).

Lehmann, 2004). These inertial and aerodynamic forces bend and twist the wings during the flapping motion, resulting in passive shape variations that may affect many aspects of flight performance.

The relative share of the inertial forces in the total normal force depends on the mass distribution, wing kinematics and other parameters affecting aerodynamic forces. There are many reports in which the inertial forces are higher than the aerodynamic forces (Lehmann and Dickinson, 1997; Daniel and Combes, 2002; Singh and Chopra, 2007), while other studies have concluded the opposite (Sun and Tang, 2002). The inertial forces may be simulated or estimated by analytical methods, while experimental methods can be used as well (Ames, 2001; Maybury and Lehmann, 2004; Singh and Ramasamy, 2005; Isaac et al., 2006). Singh and Ramasamy (2005) have also developed theoretical methods to calculate the inertial forces. A customary measuring technique involves using a vacuum container and a brass rod substituted for the wing. An accelerometer installed on the wing can also measure its acceleration.

Here, we measure the inertial forces by removing the wing's cover. We have added an equivalent point mass to the wing structure to compensate for this effect. We can measure the inertial forces due to the wing. Our simple calculation shows that in the worst case, the aerodynamic force of this wing without cover is only about 2.5% of the inertial forces (since the ribs are very thin). We also note that when the cover is removed from the wing, the kinematics of the wing will change slightly, which is neglected here. Fig. 8 shows the results, and similar results are found for other frequencies. The inertial forces are periodic with a frequency similar to that of the flapping motion. Fig. 9 shows the power consumption for covered and uncovered wing motions. The inertial share of the power consumption with respect to the total power is much lower; in fact, this power consumption is due to losses in all of the electronic and mechanical mechanisms in this system, and the net inertial effect is probably quite negligible. In this case, there is no net work performed on the wing. In other words, the inertial forces act like conservative force fields. The harmonic change in the power consumption is either due to the inertial effects or the residual aerodynamics of the uncovered wings. For the inertial forces, the average value of this harmonic function is close to zero.

8.3. Input power

The power consumption for wing flapping motion is a function of the flapping frequency. All six different wings of types A and B were tested in no-wind conditions, and the results are shown in Fig. 10. As expected, the input power increases monotonically with respect to the flapping frequency. A curve fit of this data for type A shows that the energy consumption is proportional to the square of the frequency. According to this figure, wing A1, which is the most flexible wing, has the lowest power consumption. Later, we will investigate the thrust production of different wings, and we will see that the most flexible wing has the lowest thrust production, but the specific power consumption of the flexible wings

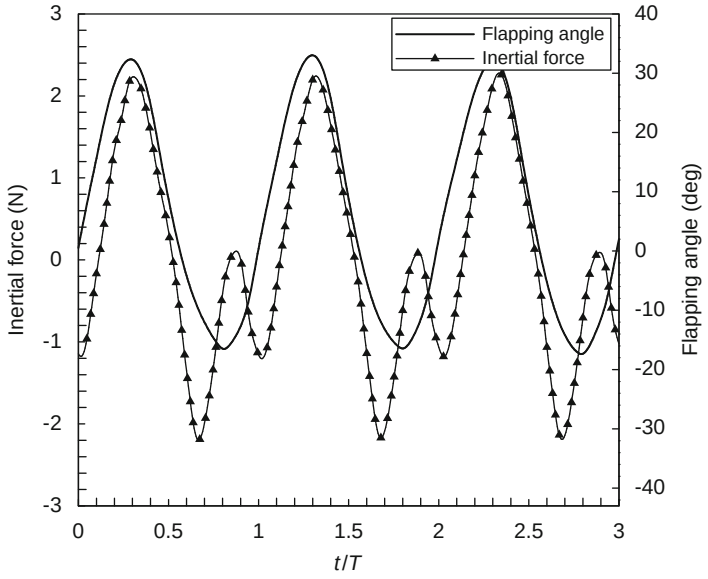

Fig. 8. Inertial force for uncovered wing A2 (5.2 Hz flapping frequency).

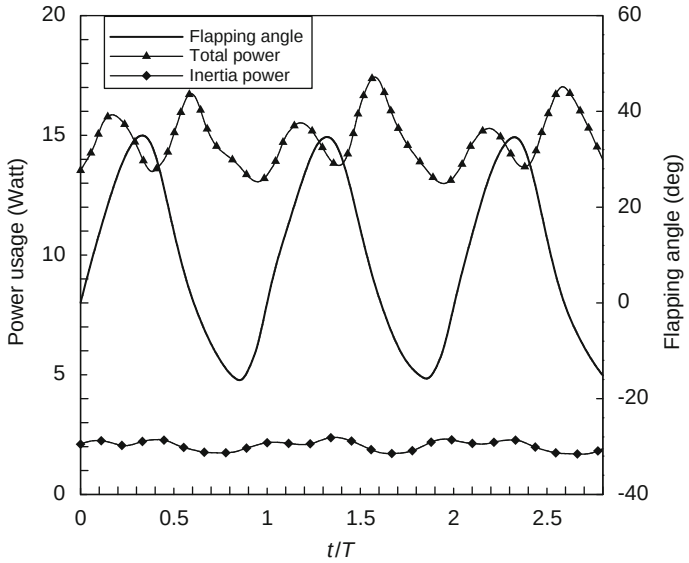

Fig. 9. Comparison of the power consumption for total forces and the inertial force (5 Hz flapping frequency).

is also the lowest. As shown in Fig. 10, the energy consumptions of the different wings types are also different. The main differences between these two wing types are their mass and area. The mass of the smaller wings, type A, is between 13.9 and 19.3 g, while for type B, it is 20.8 g. Unlike in Hong (2006), we expect that the effect of the wing mass is negligible, and the power consumption difference is mainly due to the aerodynamic effect of the different wing areas.

8.4. Thrust

Fig. 11 shows the temporal thrust variation in a no-wind situation for wing 2 of type A, flapping at a frequency of 5 Hz. Fig. 2(b) shows a snapshot taken by the high speed camera, which shows the wing deflection at point P in Fig. 11. This point corresponds to the highest velocity in the downstroke, which corresponds to the highest thrust value.

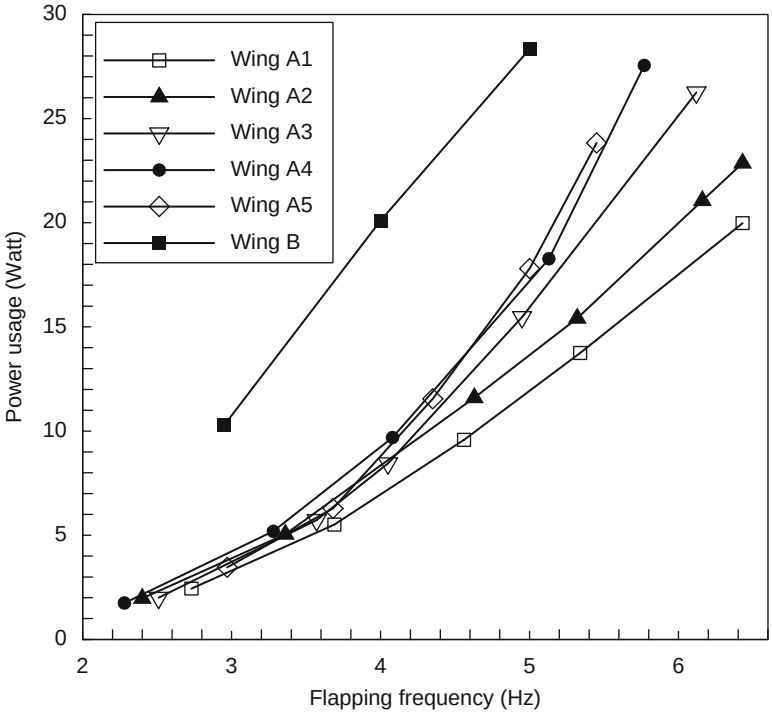

Fig. 10. The input power for various wings as a function of the flapping frequency.

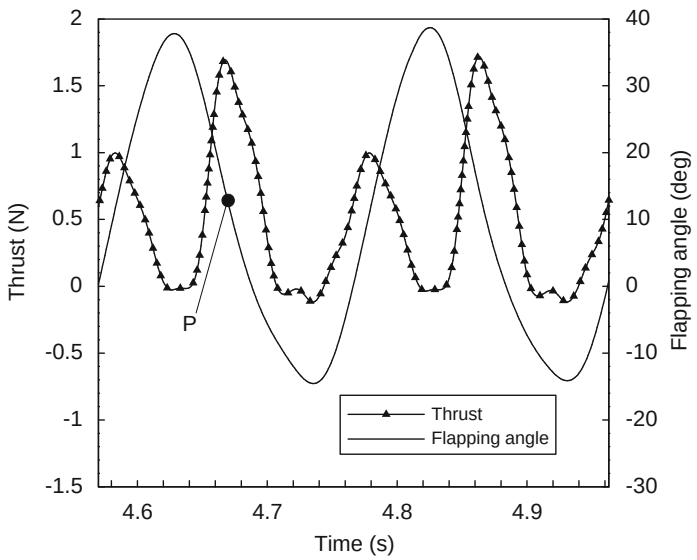

Fig. 11. Thrust variation of wing 2 (type A) for 5 Hz flapping.

Obviously, the thrust frequency is almost twice the flapping frequency, i.e., the wing will produce positive thrust on both the down and upstrokes.

Fig. 12 reports the average thrust variation as a function of flapping frequency for the same wing. Overall, the average thrust is proportional to the frequency at a power of 1.5–1.7. The thrust productions of the different wings are very similar, with a slight decrease for higher twisting flexibility, especially at higher frequencies.

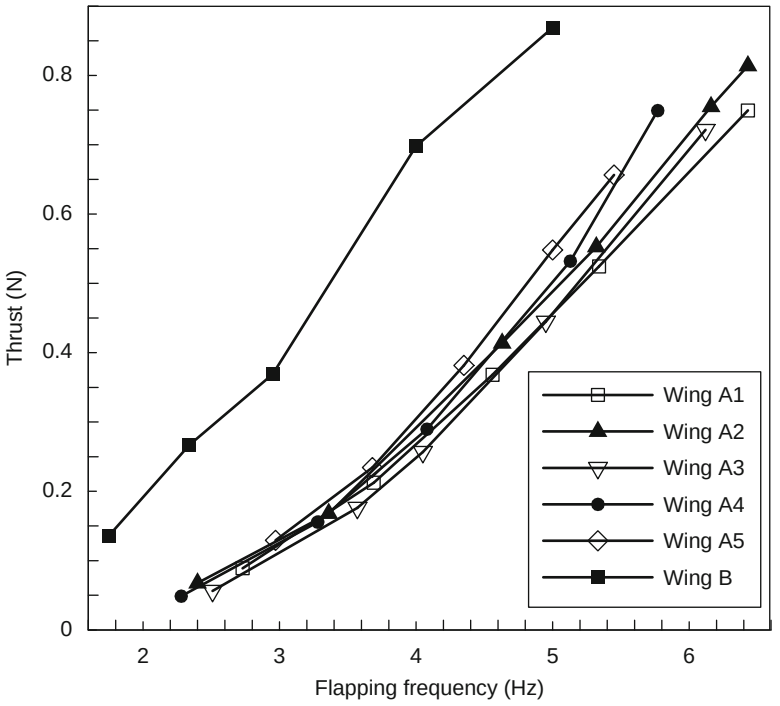

Fig. 12. Average thrust versus flapping frequency.

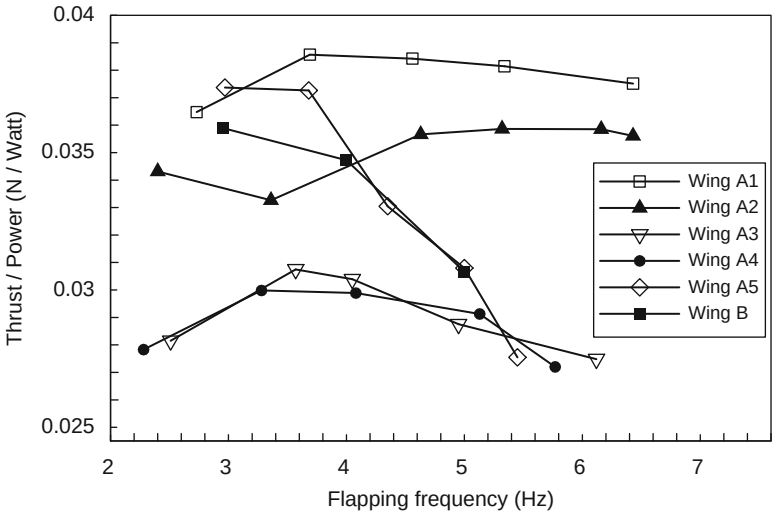

Fig. 13. Wing flapping thrust to power ratio.

One of the most important performance indexes is the thrust-to-power ratio (Bilyk, 2000; Frampton et al., 2002; Papadopoulos, 2003; Heathcote et al., 2004), which shows the overall efficiency of the wing. Fig. 13 shows this ratio for a variety of wings and excitation frequencies. Although wing A5 produces the highest thrust, wing A1 possesses the maximum thrust-to-power ratio. Since we aim to increase the flight endurance of this machine, this figure helps to find the optimum configuration. This figure shows that the performance of wing A1 is about 30% better than that of wings A3 and A4, and it is also fairly better than that of configurations A2 and A5.

For devices in hover conditions, the actuator disk theory (Shyy et al., 2008) shows that the power scales with the thrust at a power of 1.5. Thus, a figure of merit is power/(thrust)$^{1.5}$ or thrust/(power)$^{2/3}$. Fig. 14 shows the power as a

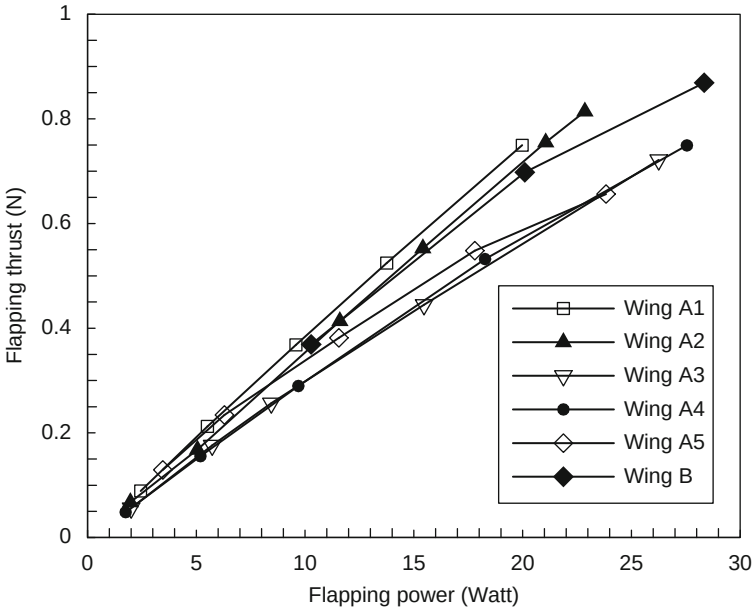

Fig. 14. Power as a function of thrust for wings A and B.

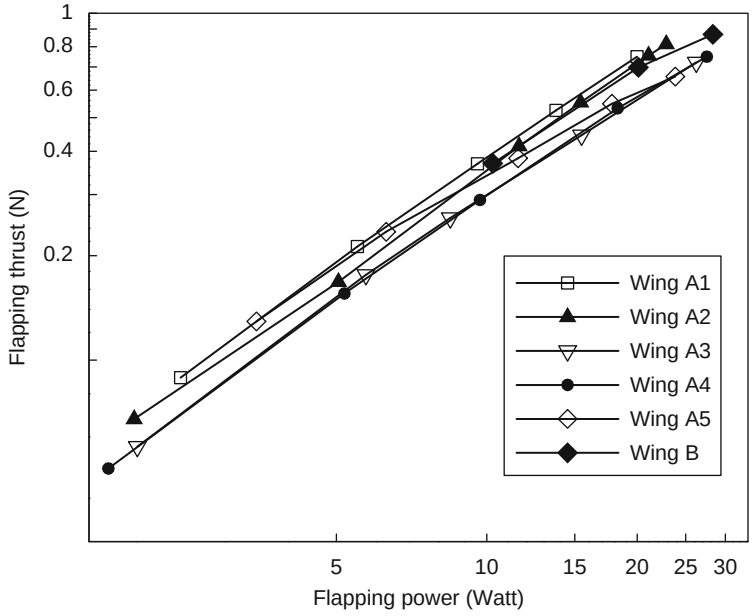

Fig. 15. Logarithm of thrust versus logarithm of power.

function of thrust for wings A and B. The two wing types (A and B) appear to behave quite differently when viewed in Figs. 10 and 12. However, as shown in Fig. 14, the performances of the two wing types actually reduce to a relatively smooth curve, which behave very much as would be predicted by the actuator disk theory. Plotted in this way, one can see that the frequency is somewhat unimportant; the power is more strongly related to the thrust in a monotonic, but not linear, way. For the different wings studied, this number varies between 0.98 and 1.1 (Fig. 15). Based on our experimental results, we emphasize that the generalization of the actuator disk theory by researchers such as Ellington

(1984) is, at most, only valid for rigid wings, and for flexible wings; the power varies by a power of about 1.0 of the thrust. Finally we observe that power is a function of required thrust, and we can optimize the thrust/power ratio by up to 30%.

9. Conclusion

In this work, a systematic method is used to analyze the aeroelastic performance of a flapping machine. An experimental set-up is presented that allows us to measure the aerodynamic forces under no-wind conditions, and a high speed camera is also utilized to observe the deformations of different wings. Many different wings of two general types were designed and fabricated, and their power consumption, normal and axial forces and inertial forces were measured.

Power consumption is the lowest for the more flexible wings, and both the thrust and power increase with increasing flapping frequency. More flexible wings produce about 20% lower thrust for high frequencies (around 5–6 Hz). Using an uncovered wing, inertial forces were independently measured. The inertial part of the power consumption is found to be negligible with respect to the part related to the work of the aerodynamic forces. The frequency of the thrust forces is twice the flapping or lifting frequencies. Finally, for many different designs, the thrust-to-power ratio was measured as a performance index to determine the optimum structural configuration that provides the highest flight endurance.

In fact, as our high speed camera shows, temporal wing deformation is the basis of force generation, and an appropriate structural design may result in a more appropriate deformation, which results in a higher lift and thrust while consuming less energy. Therefore, we found a more appropriate match between structural flexibility and aerodynamic force generation in our optimum wing. In this way, the overall wing performance is improved by about 30%. Based on our experimental results, we emphasize that the generalization of the actuator disk theory by researchers such as Ellington (1984) is, at most, only valid for rigid wings, and for flexible wings, the power varies by the thrust to a power of about 1.0.

Acknowledgements

The authors would like to acknowledge the continued support of the Sharif University of Technology Research Deputy and Aerospace Engineering Department. We also appreciate the useful comments of the reviewers of this paper, which resulted in the inclusion of additional data related to Figs. 8 and 14.

References

Ames, R.G., 2001. On the flowfield and forces generated by a rectangular wing undergoing moderate reduced frequency flapping at low Reynolds number. Ph.D. Thesis, Georgia Institute of Technology.

Bilyk, D.J., 2000. The development of flapping wings for a hovering micro air vehicle. Masters of Applied Science Thesis, University of Toronto.

Bruce, N., 1997. Micro air vehicles hold great promise. Challenges, Aviation Week & Space Technology, 14 April 1997, 67–68.

Combes, S.A., Daniel, T.L., 2003. Into thin air: contributions of aerodynamic and inertial-elastic forces to wing bending in the hawkmoth manduca sexta. The Journal of Experimental Biology 206, 2999–3006.

Daniel, T., Combes, S., 2002. Flexing wings and fins: bending by inertial or fluid dynamic forces? Integrative and Comparative Biology 42, 1044–1049.

Ebrahimi, A., Mazaheri, K., 2006. Strip theory method for ornithopter wing aerodynamic analysis. In: 10th Fluid Dynamics Conference, Yazd, Iran.

Ebrahimi, A., Mazaheri, K., 2008. Aerodynamic analysis of a flapping wing in 3D unsteady inviscid flow. In: 16th ISME2008 Conference, Kerman, Iran.

Ebrahimi, A., Karimian, S., Shidaei, A., Okhovat, S., Dehghadani, M., 2005. Primarily design of TADBIR ornithopter. Aerospace Research Centre, Sharif University of Technology, TR-01-A1-10.

Ellington, C.P., 1999. The novel aerodynamics of insect flight: applications to micro-air vehicles. The Journal of Experimental Biology 202, 3439–3448.

Ellington, C.P., 1984. The aerodynamics of hovering insect flight: V. A vortex theory. Philosophical Transactions of the Royal Society of London, Series, B 305, 115–144.

Frampton, K.D., Goldfarb, M., Monopoli, D., Cveticanin, D., 2002. Passive aeroelastic tailoring for optimal flapping wings. In: Mueller, T. (Ed.), Fixed and Flapping Wing Aerodynamics for Micro Air Vehicle Applications, Chapter 21, AIAA Progress in Aerospace Science Series.

Heathcote, S., Martin, D., Gursul, I., 2004. Flexible flapping wing propulsion at zero freestream velocity. AIAA Journal 42 (11), 2196–2204.

Ho, S., Nassef, H., Pornsinsirirak, N., Tai, Y.C., Ho, C.M., 2003. Unsteady aerodynamics and flow control for flapping wing flyers. Progress in Aerospace Sciences 39 (8), 635–681.

Hong, Y.S., 2006. An experimental study of spanwise flow effects on lift generation in flapping wings. Ph.D. Thesis, University of Dayton.

Isogai, K., Harino, Y., 2007. Optimum aeorelastic design of a flapping wing. Journal of Aircraft 44 (6), 2040–2048.

Isaac, K.M., Colozza, A., Rolwes, J., 2006. Force measurements on a flapping and pitching wing at low Reynolds numbers. AIAA Paper 2006-450.

Kim, S.W., Jang, L.H., Kim, M.H., Kim, J.S., 2003. Power-driven ornithopter piloted by remote controller. Patent No: US 6,550,716 B1.

Lehmann, F.O., Dickinson, M.H., 1997. The changes in power requirements and muscle efficiency during elevated force production in the fruit fly drosophila melanogaster. The Journal of Experimental Biology 200, 1133–1143.

Maglasang, J., Isogai, K., Goto, N., 2006. Aerodynamic study and mechanization concept for flapping-wing micro aerial vehicles. Memoirs of the Faculty of Engineering, Kyushu University 66 (1).

Maybury, W.J., Lehmann, F.O., 2004. The fluid dynamics of flight control by kinematic phase lag variation between two robotic insect wings. The Journal of Experimental Biology 207, 4707–4726.

Mazaheri, K., Molaverdikhani, K., Ebrahimi, A., 2007. Competitive environment assessment by market foresighting in MAVs industry. In: The 6th Iranian Aerospace Society Conference, K.N. Toosi University of Technology.

Mazaheri, K., Setayeshgar, A., Ebrahimi, A., 2008. Dynamic simulation of propulsion system of an ornithopter. In: Proceeding of ICETAEST, India.

Papadopoulos, J., 2003. An experimental investigation of the geometric characteristics of flapping-wing propulsion for a micro air vehicle. Master's Thesis, Naval Postgraduate School, Monterey, California.

Poelma, C., Dickson, W.B., Dickinson, M.H., 2006. Time-resolved reconstruction of the full velocity field around a dynamically-scaled flapping wing. Experiments in Fluids 41, 213–225.

Shyy, W., Berg, M., Ljungqvist, D., 1999. Flapping and flexible wings for biological and micro air vehicles. Progress in Aerospace Science 35 (5), 455–505.

Shyy, W., Lian, Y., Tang, J., Viieru, D., Liu, H., 2008. Aerodynamics of Low Reynolds Number Flyers. Cambridge University Press.

Sibilski, K., Pietrucha, J., Zlocka, M., 2007. The comparative evaluation of power requirements for fixed, rotary, and flapping wings micro air vehicles, AIAA Paper 2007-6498.

Singh, B., Ramasamy, M., 2005. Insect-based flapping wings for micro hovering air vehicles: experimental investigations. American Helicopter Society International Specialists Meeting on Unmanned Rotorcraft, Phoenix, AZ, USA.

Singh, B., Chopra, I., 2007. An aeroelastic analysis for the design of insect-based flapping wings. AIAA Paper 2007-1757.

Smith, M.J.C., 1996. Simulating moth wing aerodynamics: towards the development of flapping-wing technology. AIAA Journal 34 (7), 1348–1355.

Sun, M., Tang, J., 2002. Lift and power requirements of hovering flight in drosophila virilis. The Journal of Experimental Biology 205, 2413–2427.